Supplementary Document for the Manuscript Entitled "HT-LIP Model based Robust Control of Quadrupedal Robot Locomotion under Unknown Vertical Ground Motion"

Amir Iqbal, Sushant Veer, Christopher Niezrecki, and Yan Gu

I. Introduction

This document supplements the results presented in our paper titled "HT-LIP Model based Robust Control of Quadrupedal Robot Locomotion under Unknown Vertical Ground Motion".

A. Notations

The following notations are used in this supplementary document. The notation $|\ .\ |$ represents the absolute value function of a real scalar. For real vectors and matrices, the component-wise absolute value function is also represented by $|\ .\ |$, with abuse of notation. The 2-norm of a vector is denoted by $\|\ .\ \|$. The infinity norm of a vector is denoted by $\|\ .\ \|_\infty$. For a matrix $\mathbf{A}$, the infinity norm is defined as $\|\mathbf{A}\|_\infty = \max_i \left(\sum_j |\mathbf{A}_{ij}|\right)$, where $\mathbf{A}_{ij}$ is the element of $\mathbf{A}$ at the intersection of the i^{th} row and j^{th} column. For brevity, the following notations from the main manuscript are used: $\star|_n^- := \star(\tau_n^-)$ and $\star|_n^+ := \star(\tau_n^+)$, where τ_n^- and τ_n^+ are the time instants just before and after the switching time τ_n.

B. Abbreviations

This supplementary file uses the following abbreviations:

Abbreviation	**Description**
CoM	Center of mass.
DRS	Dynamic rigid surface.
DOF	Degree of freedom.
LIP	Linear inverted pendulum.
HT-LIP	Hybrid time-varying LIP.
QP	Quadratic program.
S2S	Step-to-step.

II. Proofs of Theorem 1 and 3

This section presents the full proofs of Theorems 1 and 3 in Sec. III ("HT-LIP based Footstep Planning") of the main paper.

This work was supported by the National Science Foundation under Grants CMMI-1934280 and CMMI-2046562 and by the Office of Naval Research under Grant N00014-21-1-2582. A. Iqbal and C. Niezrecki are with the Department of Mechanical Engineering, University of Massachusetts Lowell, Lowell, MA 01854, U.S.A. amir_iqbal@student.uml.edu and christopher_niezrecki@uml.edu. S. Veer is with NVIDIA Research, Santa Clara, CA 95051, U.S.A. sveer@nvidia.com. Y. Gu is with the School of Mechanical Engineering, Purdue University, West Lafayette, IN 47907, U.S.A. yangu@purdue.edu. Corresponding author: Y. Gu.

A. Proof of Theorem 1

This subsection provides the full proof of Theorem 1 based on the Lyapunov stability analysis on the origin of the closed-loop error dynamics.

1) Closed-loop error dynamics: Based on the HT-LIP model in (3) and the proposed discrete footstep control law in (5) of the main paper, the hybrid model of the closed-loop error system can be readily obtained as:

$$\begin{cases} \dot{\mathbf{e}} = \boldsymbol{\alpha}(t)\mathbf{e} & \text{if } t \neq \tau_n^-, \\ \mathbf{e}|_n^+ = (\mathbf{I} + \boldsymbol{\beta}\mathbf{K})\mathbf{e}|_n^- & \text{if } t = \tau_n^-, \end{cases} \tag{1}$$

where $n \in \mathbb{N}$. Recall that $\mathbf{e}$ is the tracking error state of the HT-LIP model and defined as $\mathbf{e} := [e, \dot{e}]^T$ with e the difference between the actual CoM position and the desired one. Also, recall that $\boldsymbol{\alpha}(t) := \begin{bmatrix} 0 & 1 \\ f(t) & 0 \end{bmatrix}$ with $f(t) := \frac{\ddot{z}_s(t)+g}{z_0}$, $\mathbf{I}$ is an identity matrix with a proper dimension, $\boldsymbol{\beta} := [-1,\ 0]^T$, and $\mathbf{K}$ is the feedback footstep control gain.

The S2S dynamics of the closed-loop error system are given in (6) of the main paper and listed below for the convenience of reference:

$$\mathbf{e}|_{n+1}^- = \mathbf{A}_{d,n}\mathbf{e}|_n^-. \tag{2}$$

Recall that $\mathbf{A}_{d,n}$ is the state-transition matrix of the S2S error system.

2) Lyapunov function candidate V: We consider a Lyapunov function candidate defined as $V(\mathbf{e}) := \frac{1}{2}\|\mathbf{e}\|^2$. According to the existing stability theory [1] of general discrete-time systems that include the S2S error dynamics in (2), the error dynamics are asymptotically stable if: (i) $V(\mathbf{e})$ satisfies the positive definiteness and boundedness conditions mentioned in [1] and (ii) $V(\mathbf{e}|_n^-)$ strictly decreases as n increases. It can be readily proven that condition (i) is met for the selected Lyapunov function candidate V. The rest of this subsection shows that V meets condition (ii) if the stability condition in Theorem 1 holds.

3) Boundedness of error state norm: To prove Theorem 1, we first establish the boundedness of the norm of the error state at the $(n+1)^{\text{th}}$ switching instant, i.e., $\left\|\mathbf{e}|_{n+1}^-\right\|$, in terms of $\left\|\mathbf{e}|_n^-\right\|$, as summarized in Lemma 1 later.

To introduce Lemma 1, we utilize a supreme model of the HT-LIP, which is introduced in Sec. III-B1 of the main paper and revisited here for convenience of reference. The supreme model of the continuous-time portion of the hybrid error system, i.e., $\dot{\mathbf{e}} = \boldsymbol{\alpha}(t)\mathbf{e}$, is given by:

$$\ddot{\bar{e}} = \bar{f}_n \bar{e}, \tag{3}$$

where $\bar{e}$ is the solution of (3), and the positive, constant parameter $\bar{f}_n$ is defined as $\bar{f}_n \geq \sup f(t)$ on $t \in (\tau_n, \tau_{n+1}]$.

Recall that $\bar{\boldsymbol{\Phi}}(\bar{f}_n; \tau_{n+1}^-, \tau_n^+)$ represents the state-transition matrix of the supremum time-invariant model in (3) on $t \in (\tau_n^+, \tau_{n+1}^-]$. Also, recall $\bar{\boldsymbol{\Phi}}(\bar{f}_n; \tau_{n+1}^-, \tau_n^+) = \bar{\boldsymbol{\Phi}}(\bar{f}_n; \Delta\tau_{n+1}, 0)$, where $\Delta\tau_n$ is defined as the duration of the n^{th} continuous phase and $\Delta\tau_n := \tau_{n+1} - \tau_n$.

*Lemma 1 (**Boundedness of error state norm**):* Consider assumptions (A1) and (A2) given in the main paper and the S2S error dynamics in (2). Recall $a_{d,n} := \|\bar{\mathbf{A}}_{d,n}\|_\infty := \|\bar{\boldsymbol{\Phi}}(\bar{f}_n; \Delta\tau_n, 0)(\mathbf{I} + \boldsymbol{\beta}\mathbf{K})\|_\infty$. Then, for all $n \in \mathbb{N}$, the following inequality holds

$$\left\| \mathbf{e}|_{n+1}^- \right\| \leq a_{d,n} \left\| \mathbf{e}|_n^- \right\|. \tag{4}$$

Proof: We prove Lemma 1 by first establishing the bounds on the error state $\mathbf{e}$ during $t \in [\tau_n^+, \tau_{n+1}^-]$ based on the time-varying error dynamics model $\ddot{e} = f(t)e$ (i.e., $\dot{\mathbf{e}} = \boldsymbol{\alpha}(t)\mathbf{e}$). Since this error model is time-varying, we consider its time-invariant supremum system given in (3) to establish the needed error bound.

Note that $f(t)$ is positive for all $t \in \mathbb{R}^+$. Then, according to the results of the Strong Comparison Theorem in Sec. 2 of [2], the solutions e and $\bar{e}$ satisfy the following inequality for all $t \in (\tau_n, \tau_{n+1}]$

$$|e(t)| \leq |\bar{e}(t)| \tag{5}$$

when they share the same initial condition of $e(\tau_n^+) = \bar{e}(\tau_n^+)$.

By using (5) and the state-transition matrix $\bar{\boldsymbol{\Phi}}(\bar{f}_n; \tau_{n+1}^-, \tau_n^+)$, the error state $\mathbf{e}|_{n+1}^-$ is bounded as:

$$\left| \mathbf{e}|_{n+1}^- \right| \leq \left| \bar{\boldsymbol{\Phi}}(\bar{f}_n; \tau_{n+1}^-, \tau_n^+) \mathbf{e}|_n^+ \right|. \tag{6}$$

Next, we apply the discrete switching map in (1) to the equation above and obtain:

$$\left| \mathbf{e}|_{n+1}^- \right| \leq \left| \bar{\boldsymbol{\Phi}}(\bar{f}_n; \Delta\tau_{n+1}, 0)(\mathbf{I} + \boldsymbol{\beta}\mathbf{K}) \mathbf{e}|_n^- \right|. \tag{7}$$

Recall that the state-transition matrix of the complete hybrid supreme model is given by:

$$\bar{\mathbf{A}}_{d,n} := \bar{\boldsymbol{\Phi}}(\bar{f}_n; \Delta\tau_n, 0)(\mathbf{I} + \boldsymbol{\beta}\mathbf{K}). \tag{8}$$

With the state-transition matrix defined as in (8), we can rewrite the right-hand side of the inequality in (7) as:

$$\left| \mathbf{e}|_{n+1}^- \right| \leq |\bar{\mathbf{A}}_{d,n} \mathbf{e}|_n^-|. \tag{9}$$

Given the sub-multiplicative property of $|\bar{\mathbf{A}}_{d,n} \mathbf{e}|_n^-|$, (9) becomes:

$$\left| \mathbf{e}|_{n+1}^- \right| \leq \left| \bar{\mathbf{A}}_{d,n} \right| \left| \mathbf{e}|_n^- \right|. \tag{10}$$

Adding an induced matrix norm $\|.\|$ to both sides of (10) and using the properties of $\|.\|$, we get:

$$\begin{aligned} \left\| \mathbf{e}|_{n+1}^- \right\| &\leq \left\| (|\bar{\mathbf{A}}_{d,n}| |\mathbf{e}|_n^-|) \right\| \leq \left\| \bar{\mathbf{A}}_{d,n} \right\|_\infty \left\| \mathbf{e}|_n^- \right\| \\ &= a_{d,n} \left\| \mathbf{e}|_n^- \right\|, \end{aligned} \tag{11}$$

which completes the proof. ■

4) Proof of Theorem 1: Based on Lemma 1, the proof of Theorem 1 is given as follows:

Proof: Using (4) in Lemma 1, we analyze an upper bound of the change in the Lyapunov function $\Delta V(\mathbf{e}|_n^-)$ across two adjacent foot landings as:

$$\begin{aligned} \Delta V(\mathbf{e}|_n^-) &:= V(\mathbf{e}|_{n+1}^-) - V(\mathbf{e}|_n^-) = \frac{1}{2} \left\| \mathbf{e}|_{n+1}^- \right\|^2 - \frac{1}{2} \left\| \mathbf{e}|_n^- \right\|^2 \\ &\leq \frac{1}{2} a_{d,n}^2 \left\| \mathbf{e}|_n^- \right\|^2 - \frac{1}{2} \left\| \mathbf{e}|_n^- \right\|^2 =: -\sigma_n \left\| \mathbf{e}|_n^- \right\|^2, \end{aligned} \tag{12}$$

where σ_n is defined as $\sigma_n := \frac{1}{2}(1 - a_{d,n}^2)$. If the positive variable $a_{d,n}$ satisfies $a_{d,n} < 1$ for all $n \in \mathbb{N}$, then $-\sigma_n < 0$ holds on $n \in \mathbb{N}$. Accordingly, the Lyapunov function V satisfies all the sufficient stability conditions described in Sec. II-A2. This completes the proof. ■

B. Proof of Theorem 3

Proof: Minimizing the cost function $J(\mathbf{K})$ leads to the minimization of the variable $a_{d,n}$ while the physical feasibility and asymptotic stability of the closed-loop HT-LIP system are guaranteed by enforcing the constraint $\mathbf{E}\mathbf{K}^T < \mathbf{d}$. Hence, the optimal solution to the QP problem corresponds to the optimal convergence rate, feasibility, and stability. ■

III. Middle Layer: Full-Order Model Based Trajectory Generation

This section explains the middle layer of the proposed control framework introduced in Sec. III of the main manuscript.

The essence of the proposed middle layer is the commonly adopted trajectory interpolation based on the robot's full-order kinematics model [3]–[5]. Specifically, the middle layer translates the desired CoM and footstep locations, which are generated by the HT-LIP based footstep planner (i.e., the higher layer), into the desired full-body trajectories for all DOFs of the robot. This translation also respects the model simplifying assumptions underlying the proposed HT-LIP model. By enforcing both the desired trajectories generated by the higher layer and the HT-LIP model assumptions, the middle layer can effectively reduce the discrepancy between the HT-LIP model and the actual robot dynamics.

A. Control Variable Selection

As discussed in the main paper, a quadrupedal robot (e.g., Unitree's Go1 robot) during trotting is typically underactuated with 13 DOFs and 12 independent actuators. Therefore, a full-body controller can directly command twelve independent position or orientation variables.

In this study, the full-order trajectories we choose to directly control are the six-dimensional (6-D) base pose (i.e.,

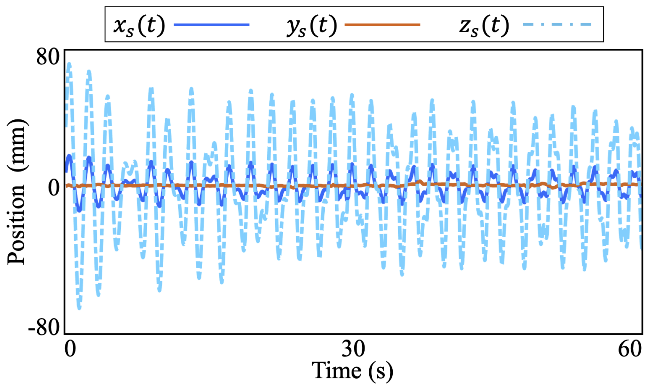

Fig. 1. Ground-truth position trajectory of the point on the DRS around which the robot performs the trotting gait during the unknown pitch movement (HC1) of the DRS.

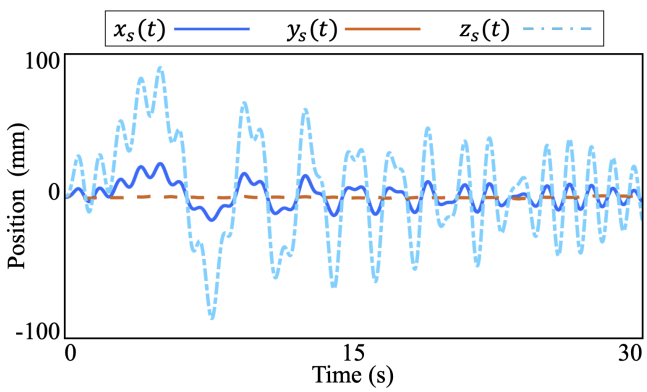

Fig. 2. Ground-truth position trajectory of the point on the DRS around which the robot performs the trotting gait during the unknown pitch movement (HC2) of the DRS.

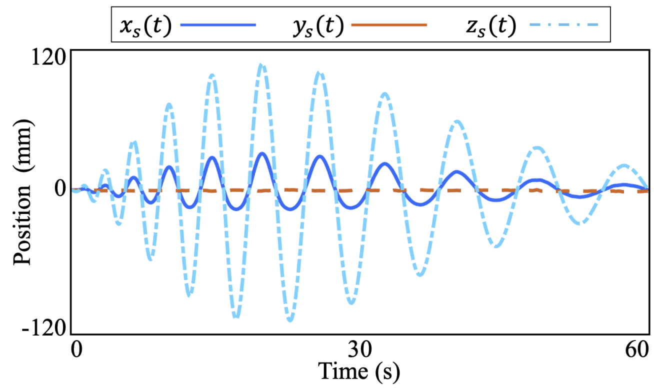

Fig. 3. Ground-truth position trajectory of the point on the DRS around which the robot performs the trotting gait during the unknown pitch movement (HC3) of the DRS.

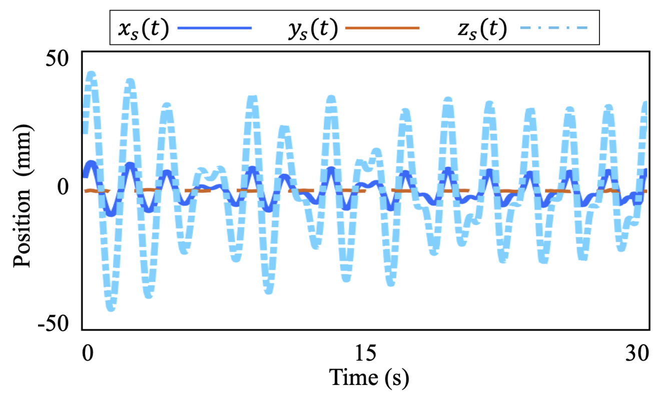

Fig. 4. Ground-truth position trajectory of the point on the DRS around which the robot performs the trotting gait during the unknown pitch movement (HC5) of the DRS.

position and orientation) and the 3-D positions of the two swing feet. Given that the CoM of a typical quadruped is close to its base/trunk center, the desired CoM trajectory produced by the higher layer is assigned as the desired base trajectory of the quadruped. Directly commanding the base position trajectories allows the indirect tracking of the desired CoM trajectories, and controlling the swing foot positions can ensure the robot reliably executes the desired foot-landing time instants.

1) Base pose trajectory generation: The vector of the robot's desired base trajectories is given as: $\mathbf{h}_{b,d} = [x_{b,d}, y_{b,d}, z_{b,d}, \phi_{b,d}, \theta_{b,d}, \psi_{b,d}]^T$, where $(x_{b,d},\ y_{b,d},\ z_{b,d})$ and $(\phi_{b,d},\ \theta_{b,d},\ \psi_{b,d})$ are the base position and orientation (i.e., roll, pitch, and yaw angles) with respect to the world frame, respectively.

The desired horizontal base trajectories $x_{b,d}$ and $y_{b,d}$ are provided by the higher-layer footstep planner. To respect assumption (A3) given in the main manuscript, the desired base height $z_{b,d}$ relative to the support point of the HT-LIP is designed to be equal to the constant z_0; that is, $z_{b,d} = z_0$.

The desired base yaw trajectory $\psi_{b,d}$ is planned based on the user-specified yaw rate $\omega_{b,d}$. Additionally, for simplicity and without loss of generality, the desired base roll and pitch angles, $\phi_{b,d}$ and $\theta_{b,d}$, are both set to zero for maintaining a steady trunk posture.

2) Swing foot position trajectory generation: As mentioned earlier, there are always two legs swinging in the air during quadrupedal trotting. The desired maximum height of the two swing feet is set as a kinematically feasible value. Meanwhile, the desired horizontal swing foot trajectories are designed as Bézier curves [6] to agree with the desired footstep length generated by the higher-layer footstep planner, the actual swing foot locations at the beginning of the given continuous phase, and the desired continuous-phase duration.

IV. Full-Order Model Based Closed-Loop Stability Analysis

This section provides the closed-loop stability analysis for the unactuated subsystem of the hybrid, time-varying, full-order robot model under the proposed hierarchical control framework.

As mentioned in Sec. III of the main manuscript, the trotting quadruped of interest to this study is underactuated. Since its degree of underactuation is one, its underactuated dynamics are two-dimensional, which can be represented by the dynamics of the forward CoM position and velocity (i.e., $\mathbf{X}$) associated with the full-order robot model. The actuated dynamics of the full-order model correspond to the base pose and the swing foot position trajectories that are directly driven by the lower-layer controller. Note that for the actual robot and its full-order model, the CoM and the base center

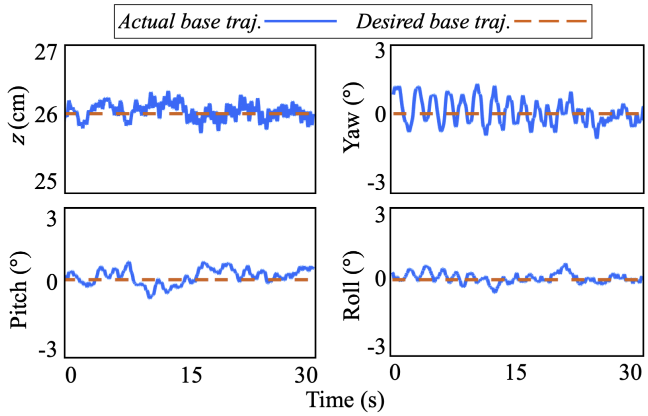

Fig. 5. Desired and actual base trajectories under the hardware experiment case (HC2). The small tracking errors indicate stable robot trotting.

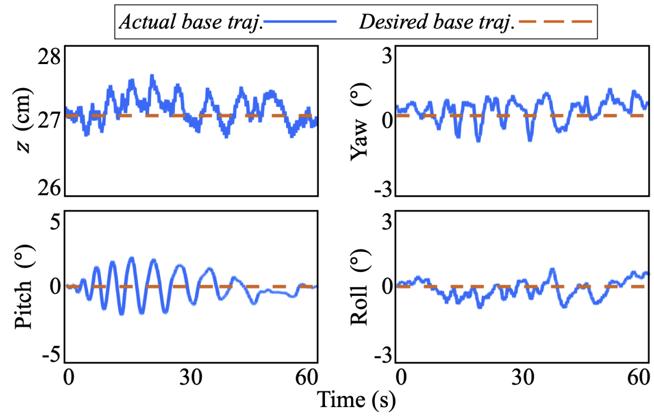

Fig. 7. Desired and actual base trajectories under the hardware experiment case (HC3). The small tracking errors indicate stable robot trotting.

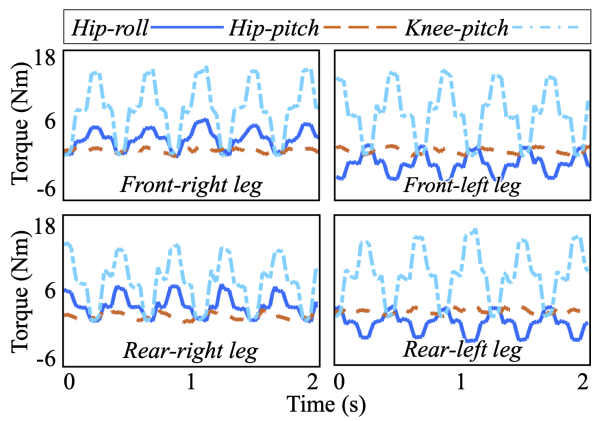

Fig. 6. Torque profiles under the hardware experiment case (HC2), all of which respect the robot's individual actuator limit of 22.5 Nm.

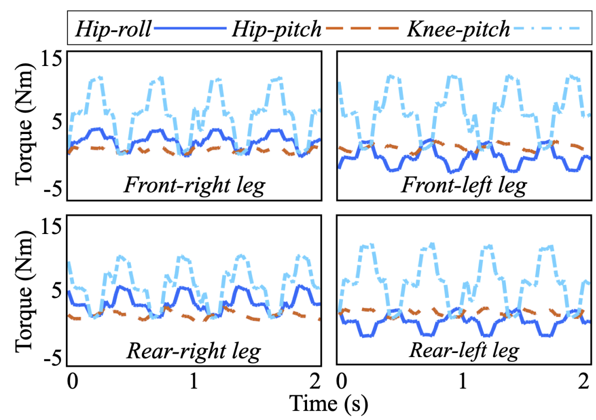

Fig. 8. Torque profiles under the hardware experiment case (HC3), all of which respect the robot's individual actuator limit of 22.5 Nm.

of the robot do not coincide due to the nontrivial mass of the legs.

Since the forward CoM position and velocity for the full-order model are not directly actuated, we need to explicitly analyze the stability of their dynamics. As mentioned earlier, the actual dynamics of the CoM forward position and velocity $\mathbf{X}$ can be approximated by the proposed HT-LIP model given in (3) of the main manuscript. Although the proposed HT-LIP footstep control law provably ensures the asymptotic stability of the closed-loop HT-LIP model under unknown surface motions, the stability of the closed-loop dynamics of the CoM state $\mathbf{X}$ based on the actual full-order model still needs to be analyzed. This is due to the discrepancy between the HT-LIP model and the actual dynamics of the CoM state $\mathbf{X}$.

A. S2S Error System of Actual CoM Dynamics

Based on the closed-loop error system dynamics of the HT-LIP model given in (2), the S2S error system of the actual CoM dynamics can be expressed as:

$$\mathbf{e}|_{n+1}^{-} = \mathbf{A}_{d,n}\mathbf{e}|_{n}^{-} + \mathbf{d}_n, \tag{13}$$

where $n \in \mathbb{N}$. Here the vector $\mathbf{d}_n$ represents the lumped discrepancy between the actual S2S dynamics of the CoM and the reduced-order HT-LIP model, including the ignored nonlinear term in the S2S dynamics and the difference between the desired and actual footstep locations.

B. Stability Analysis

Similar to [7], we consider the boundedness of the model discrepancy $\mathbf{d}_n$ as:

$$\|\mathbf{d}_n\| < d \quad \forall n \in \mathbb{N}, \tag{14}$$

where d is a positive constant. This boundedness assumption is reasonable for hardware implementation when the desired step duration is designed as finite (assumption (A2)) and the initial tracking error is relatively small. We denote the set of all possible values of $\mathbf{d}_n$ satisfying (14) as $\mathcal{D}$; that is, $\mathbf{d}_n \in \mathcal{D}$.

We use $\mathcal{E}$ to denote the minimum invariance set [8] such that for all $\mathbf{e}|_{n}^{-} \in \mathcal{E}$ and $\mathbf{d}_n \in \mathcal{D}$, we have $\mathbf{e}|_{n+1}^{-} \in \mathcal{E}$. Also, recall that the asymptotic stability condition for the closed-loop error system of the HT-LIP model is established in Theorem 2 of the main manuscript. Consequently, the S2S dynamics in (13) are locally stable [8], [9] if the asymptotic stability condition for the HT-LIP model in Theorem 2 is met and if the uncertainty boundedness condition in (14) holds.

V. Supplementary Hardware Experiment Results

This section reports the supplementary results of the hardware validation experiments.

Figures 1-4 show the general, aperiodic displacement profiles of a point on the DRS/treadmill near the footholds of the robot for cases (HC1)-(HC3) and (HC5), respectively.

The base trajectory tracking plots corresponding to the DRS motions (HC2) and (HC3) are illustrated in Figs. 5 and 7, respectively. The corresponding joint torque plots in Figs. 6 and 8 show that the torque trajectories are within the actuator limit of 22.5 Nm for each joint. Both the reliable base trajectory tracking and the consistent torque profiles confirm stable trotting under DRS motion cases (HC2) and (HC3).

REFERENCES

[1] J. Daafouz and J. Bernussou, "Parameter dependent lyapunov functions for discrete time systems with time varying parametric uncertainties," *Syst. Contr. L.*, vol. 43, no. 5, pp. 355–359, 2001.

[2] A. McNabb, "Comparison theorems for differential equations," *J. Math. Anal. Appl.*, vol. 119, no. 1-2, pp. 417–428, 1986.

[3] M. Focchi, A. Del Prete, I. Havoutis, R. Featherstone, D. G. Caldwell, and C. Semini, "High-slope terrain locomotion for torque-controlled quadruped robots," *Autonomous Robots*, vol. 41, no. 1, pp. 259–272, 2017.

[4] G. Bledt, M. J. Powell, B. Katz, J. Di Carlo, P. M. Wensing, and S. Kim, "MIT Cheetah 3: design and control of a robust, dynamic quadruped robot," in *Proc. IEEE/RSJ Int. Conf. Intel. Rob. Syst.*, pp. 2245–2252, 2018.

[5] A. Iqbal, S. Veer, and Y. Gu, "Analytical solution to a time-varying LIP model for quadrupedal walking on a vertically oscillating surface," *IFAC Mechatron.*, 2022, in press.

[6] E. R. Westervelt, J. W. Grizzle, C. Chevallereau, J. H. Choi, and B. Morris, *Feedback control of dynamic bipedal robot locomotion*, vol. 28. CRC press, 2007.

[7] X. Xiong and A. Ames, "3-D underactuated bipedal walking via H-LIP based gait synthesis and stepping stabilization," *IEEE Trans. Rob.*, vol. 38, no. 4, pp. 2405–2425, 2022.

[8] S. V. Rakovic, P. Grieder, M. Kvasnica, D. Q. Mayne, and M. Morari, "Computation of invariant sets for piecewise affine discrete time systems subject to bounded disturbances," in *2004 43rd IEEE Conference on Decision and Control (CDC)(IEEE Cat. No. 04CH37601)*, vol. 2, pp. 1418–1423, IEEE, 2004.

[9] L. Magni, G. De Nicolao, R. Scattolini, and F. Allgöwer, "Robust model predictive control for nonlinear discrete-time systems," *International Journal of Robust and Nonlinear Control: IFAC-Affiliated Journal*, vol. 13, no. 3-4, pp. 229–246, 2003.